Available online at www.sciencedirect.com
SCIENCE DIRECT®
Journal of Computational Physics 190 (2003) 325–345
JOURNAL OF COMPUTATIONAL PHYSICS
www.elsevier.com/locate/jcp

A new first kind boundary integral formulation for the Dirichlet-to-Neumann map in 2D

Patrick Guidotti *

Department of Mathematics, University of California, 103 Science and Technology Bldg., Irvine, CA 92697-3785, USA

Received 5 September 2002; received in revised form 12 March 2003; accepted 13 May 2003

Abstract

In this paper, we analyze the Dirichlet-to-Neumann (DtN) operator in the periodic case as a pseudodifferential operator represented through boundary integrals. We begin with some analytical results concerning the structure of the operator. In particular we exploit the freedom available in the choice of the kernel for the boundary integral representation to introduce a new logarithmic kernel for the fundamental solution of the Laplacian on a cylinder. We then use it to develop a superalgebraically convergent numerical method to compute DtN which proves very stable even for nonsmooth and large variation curves. An important step in the proposed procedure is the inversion of an integral equation of first kind. To deal with it, we introduce an efficient FFT-based preconditioner which performs well in combination with Nystrom's method and a decomposition of the operator based on "flat geometry subtraction".

Keywords: Dirichlet-to-Neumann Operator; Superalgebraic convergence; Boundary integral method; Fourier analysis; Integral equation of first kind; Preconditioning

1. Introduction

A large variety of classical problems of mathematical physics lead to systems often comprising simple potential equations in domains with nontrivial geometries and nonhomogeneous boundary data. A typical situation is given when one is interested in computing a boundary force in terms of the normal derivative of a potential for which Dirichlet data are known. This happens for fixed and moving boundary value problems in electro-magnetism, fluid dynamics and solid mechanics (cf. for instance [1,2,5,11,13]). It also naturally arises when one introduces artificial boundaries for the numerical purpose of solving problems in unbounded domains (cf. [7] for instance).

Solving the Dirichlet problem in a bounded or unbounded domain in order to compute the normal derivative of the solution on the boundary precisely defines what is known as the Dirichlet-to-Neumann

* Tel.: +1-949-824-1266; fax: +1-949-824-7993.
E-mail address: gpatrick@math.uci.edu.

0021-9991/$ - see front matter
doi:10.1016/S0021-9991(03)00277-8

map (DtN operator) in the literature, see [14]. The DtN operator is particularly easy to deal with if the domain has a simple geometry but its efficient computation rapidly becomes challenging if the domain geometry significantly deviates from a simple one. Complicated or nonsmooth geometries are very natural especially in electro-magnetic scattering problems or in free boundary problems of fluid and solid mechanics. Whence the need of finding efficient and simple ways to compute the DtN operator which are as much as possible insensitive to domain geometry. To keep the presentation short we restrict our attention to Laplace's equation only.

1.1. What is known?

There are essentially two approaches that have been taken to computing the DtN operator: perturbative pseudo-differential operator techniques and so-called boundary integral methods.

The first is perturbative in nature. It relies on an old result by Coifman and Meyer [3] which shows analytic dependence of the DtN operator on the curve/surface in a Lipschitz neighborhood of a flat curve/surface. This approach is used for instance in [5]. The nonconstant coefficient Fourier symbol for the perturbed DtN operator is developed in a power series for the function representing the curve, which in particular needs to be of graph type. By truncating the series, the actual problem is then reduced to computing a finite linear combination of compositions of multiplication operators and constant coefficient pseudodifferential operators the symbol of which can be obtained analytically. Either type of operator can then be computed efficiently in physical and in Fourier space, respectively. A recent paper by Nicholls and Reitich [14] gives a nice overview of these methods and improves on some of their features. In particular these perturbative methods tend to be numerically unstable even for smooth curves due to analytical cancellation effects in the terms of the series expansion. Nicholls and Reitich [14] show how these methods can be made more stable by eliminating cancellation effects taking into account a higher computational cost and some analytical manipulations.

The second is based on classical boundary integral representations for the solution using single and double layer potentials. This technique can be used for a variety of different problems. The knowledge of a fundamental solution for the potential equation in free space allows one to derive a relation (using Green's formula, see for instance [9]) between Dirichlet and Neumann boundary data for a harmonic function of the interior. This approach, implemented for instance in [1,2] has the advantage of applying to general curves. In particular they need not be of graph type. At the same time it prevents the use of Fourier arguments precisely because it can handle very general geometries which are not even close to being linear/circular. Another price which needs to be paid is that the integral equations have singular or weakly singular kernels, which is a real numerical issue especially for surfaces in $\mathbb{R}^3$. These methods would also profit from an improvement of their numerical stability. In [8] the authors give a nice general overview of the use of boundary integral methods in applied mathematics, especially in fluid dynamics.

1.2. What is new?

Our program is to first consider the problem of finding a satisfactory analytical representation for the DtN operator and subsequently to use it in order to obtain a good discretization. In order to do so we derive a new kernel of logarithmic type for the fundamental solution for the Laplace operator on an cylinder. With it we propose a single-layer potential boundary integral method for the computation of DtN. The procedure entails solving an integral equation of first kind. The discretized equations will inherit the ill-posedness of their continuous counterpart and suffer from the presence of singular integrals. We show how the difficulties stemming from these can be elegantly circumvented by using a boundary integral method combined with Fourier analysis, however not in a perturbative way. More specifically we propose a FFT-based preconditioner, which, combined with the standard flat geometry subtraction, eventually leads to a

superalgebraically convergent scheme for the computation of DtN. Our final product will be an accurate and stable pseudo-spectral (Fourier) boundary integral method which performs equally well for nonsmooth and/or large variation curves as it does for small variation smooth curves. The ideas can readily be applied to the analogous 3D problem but will be the topic of another paper.

The rest of the paper is organized as follows. In Section 2, we perform all the preparatory analytical work. We in particular set up a bridge between the boundary integral method and the Fourier method. In Section 3, we introduce a discretization of the analytical representations by means of Nystrom's method combined with the choice of optimal quadrature rules and with a FFT-based preconditioner. Finally Section 4 is devoted to numerical experiments in support of our theoretical claims. In Appendix A, we give a proof of the jump relation satisfied by the integral representations based on the new kernel. In Appendix B, we show how the nonconstant coefficient symbol of the general representation can be derived from the "flat" symbol.

2. Analysis of the DtN operator

In this paper, we concentrate our attention on the 2D periodic situation. More precisely we consider Laplace's equation

$$-\Delta u = 0 \quad \text{in } \Omega_\Gamma, \qquad u = g \quad \text{on } \Gamma \tag{2.1}$$

in the region Ω_Γ lying above the 1-periodic curve Γ. Although the results presented here remain valid in the case of general curves we restrict ourselves to the case of curves which can be represented as the graph of a function for the sake of simplicity. For the general case we refer to Remark 5 in Section 2.3 and the numerical experiments of Section 4 (cf. Examples 4 and 8). We propose the new kernel

$$G(x,y) = \frac{1}{2\pi}\ln\left(1 + \mathrm{e}^{-4\pi y} - 2\cos(2\pi x)\mathrm{e}^{-2\pi y}\right), \tag{2.2}$$

which is 1-periodic in the first variable, and the corresponding representation for the solution u_g of (2.1) of the form

$$u_g(z) = \int_\Gamma G(z-\tilde{z}) f(\tilde{z})\,\mathrm{d}\sigma_\Gamma(\tilde{z}), \quad z \in \Omega_\Gamma \tag{2.3}$$

in terms of an unknown boundary function f. If we assume that the curve Γ be parametrized by the 1-periodic function s, the integral (2.3) reads

$$u_g(x,y) = \int_0^1 G(x-\tilde{x}, y-s(\tilde{x})) f(\tilde{x}) \sqrt{1+s_x^2(\tilde{x})}\,\mathrm{d}\tilde{x}, \quad (x,y) \in \Omega_\Gamma. \tag{2.4}$$

Since we are eventually interested in the derivative in normal direction restricted to the boundary we assume the boundary value g has mean zero, that is,

$$\int_\Gamma g(\tilde{z})\,\mathrm{d}\sigma_\Gamma(\tilde{z}) = 0. \tag{2.5}$$

It has indeed been shown (see for instance [16]) that the kernel of DtN consists of mean zero boundary functions in a variety of functions spaces comprising $L_2(\Gamma)$ for a simple example. Assumption (2.5) also makes

$$g = \left(\int_\Gamma G(\cdot - \tilde{z}) f(\tilde{z})\,\mathrm{d}\sigma_\Gamma(\tilde{z})\right)\Big|_\Gamma$$

uniquely solvable. Let ν denote the unit outer normal to Ω. After finding the boundary function f we use (2.4) to derive a boundary integral representation of $\mathrm{DtN}(g) = \partial_\nu u_g|_\Gamma$ (the restriction might occasionally need to be understood in the sense of traces) as follows

$$\mathrm{DtN}(g)(z) = \left(\int_\Gamma \Big(\nabla G(z-\tilde{z}) | \nu(z) \Big) f(\tilde{z}) \, \mathrm{d}\sigma_\Gamma(\tilde{z}) \right) \Bigg|_\Gamma \tag{2.6}$$

or, in coordinates,

$$\mathrm{DtN}(g)(\tilde{x}) = \left(\int_0^1 K(x,\tilde{x}) f(\tilde{x}) \frac{\sqrt{1+s_x^2(\tilde{x})}}{\sqrt{1+s_x^2(x)}} \, \mathrm{d}\tilde{x} \right) \Bigg|_{y=s(x)} \tag{2.7}$$

for

$$K(x,\tilde{x}) = \partial_x s(x) \partial_x G(x-\tilde{x}, y-s(\tilde{x})) - \partial_y G(x-\tilde{x}, y-s(\tilde{x})).$$

We defined the function u_g only above the curve Γ and it is therefore clear that the above restrictions are always meant to be obtained by taking the limit from above the curve Γ. In view of the singularity of kernel (2.2) a singular interaction along the boundary curve will in fact produce a Dirac contribution as we shall see below.

2.1. Derivation of the kernel

Let us start with the trivial case, where the curve Γ is the x-axis. It is natural to look for a solution in Fourier space and, since we are focussing on the periodic case, we obviously easily obtain the standard representation for the solution of (2.1)

$$u_g(x,y) = \sum_{k=-\infty}^{\infty} \hat{g}_k \mathrm{e}^{-2\pi|k|y} \mathrm{e}^{2\pi \mathrm{i} k x} \tag{2.8}$$

in terms of the Fourier coefficients of the boundary function g. From (2.8) we can trivially compute

$$\mathrm{DtN}(g) = 2\pi \sum_{k=-\infty}^{\infty} |k| \hat{g}_k \mathrm{e}^{-2\pi|k|y} \mathrm{e}^{2\pi \mathrm{i} k x} \Bigg|_{y=0}.$$

But this is not the way we want to look at the above formulas. We actually want to take a more abstract perspective based on pseudo differential operators (ΨDOs in the sequel) techniques. If we view

$$\left(\mathrm{e}^{-2\pi|k|y} \right)_{k\in\mathbb{Z}}$$

as the symbol of a ΨDO with constant coefficients (depending on the parameter $y > 0$) we can actually compute the kernel of the corresponding convolution operator associated to (2.8) (at least for fixed y) to obtain

$$H(x,y) = \sum_{k=-\infty}^{\infty} \mathrm{e}^{-2\pi|k|y} \mathrm{e}^{2\pi \mathrm{i} k x} = \frac{2 - 2\mathrm{e}^{-2\pi y} \cos(2\pi x)}{1 + \mathrm{e}^{-4\pi y} - 2\cos(2\pi x)\mathrm{e}^{-2\pi y}} - 2, \tag{2.9}$$

where H is nothing but a harmonic function of the upper/lower half plane for which

$$\lim_{y\to 0+} H(\cdot, y) = \delta - 1 \text{ in } \mathscr{D}'_p(0,1),$$

where we introduce the space

$$\mathscr{D}'_p(0,1) = \mathscr{L}\Big(C^\infty_p(0,1), \mathbb{K}\Big)$$

of 1-periodic distributions over the line as the dual of 1-periodic test functions with its natural (locally convex) Fréchet topology. Let us introduce a 1-periodic convolution through

$$(u *_p v)(x) = \int_0^1 u(x-\tilde{x})v(\tilde{x})\,\mathrm{d}\tilde{x}, \quad x \in (0,1), \tag{2.10}$$

which is easily checked to be well-defined by thinking of u as being periodically extended outside $(0,1)$ in order to make sense of $u(x-\tilde{x})$. Alternatively, if we prefer the comfort of working solely in one periodicity interval, we can interpret the sum $x-\tilde{x}$ as a sum modulo the period. In this new notation, the unique bounded solution to the periodic Poisson equation is seen to be given by

$$u_g(x,y) = \big(H(\cdot,y) *_p f\big)(x) = \int_0^1 H(x-\tilde{x},y)f(\tilde{x})\,\mathrm{d}\tilde{x}, \tag{2.11}$$

which is nothing else but the periodic version of the well-known Poisson integral. We can therefore reinterpret the computation of DtN(g) in this case as first solving the convolution equation

$$\int_0^1 H(x-\tilde{x},0)f(\tilde{x})\,\mathrm{d}\tilde{x} = \langle \delta_{(x-\cdot)} - 1, f\rangle = g(x), \quad x \in (0,1), \tag{2.12}$$

which is trivially solved by $f = g$ (recall that g is assumed to have mean zero) and then computing

$$\partial_\nu u_g(x) = -\lim_{y\to 0}\int_0^1 \partial_y H(x-\tilde{x},y)f(\tilde{x})\,\mathrm{d}\tilde{x} = -\big(H_y(\cdot,0) *_p f\big)(x) = f(x), \tag{2.13}$$

which is a boundary representation of the derivative in normal direction of u_g. Although this is a perfectly valid analytic representation, the kernel $\partial_y H(\cdot,0)$ is unfortunately hypersingular and won't provide a viable computational recipe. With this new point of view, though, we are now able to avoid dealing with hypersingular kernels directly. Eq. (2.12) is a mere instance of a variety of other possible superpositions of harmonic functions. We can, for instance, use the alternative kernel G obtained by integrating (2.9) with respect to the y-variable. It coincides with (2.2) and is clearly again a x-periodic harmonic function. A contour plot of G is shown in Fig. 1 together with its continuous counterpart. Using (2.2) we represent the solution of Laplace's equation through

$$u_g(x,y) = \int_0^1 G(x-\tilde{x},y)f(\tilde{x})\,\mathrm{d}\tilde{x} \tag{2.14}$$

and finding f by imposing the boundary condition

$$\int_0^1 G(x-\tilde{x},0)f(\tilde{x})\,\mathrm{d}\tilde{x} = g(x), \quad x \in (0,1), \tag{2.15}$$

which is an integral equation of the first kind with a less singular kernel than (2.12) and, eventually computing

$$-\lim_{y\to 0}\int_0^1 \partial_y G(x-\tilde{x},y)f(\tilde{x})\,\mathrm{d}\tilde{x} = -\int_0^1 H(x-\tilde{x},0)f(\tilde{x})\,\mathrm{d}\tilde{x} = -f(x). \tag{2.16}$$

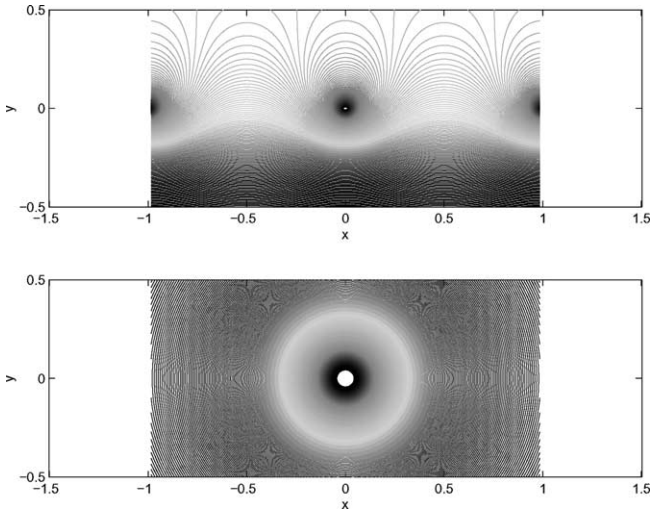

Fig. 1. A contour plot of G and $\frac{1}{\pi}\log(x^2+y^2)$.

Remark 1. Using representation (2.14) instead of (2.11) corresponds to using the fundamental solution $\frac{1}{2\pi}\ln|(x,y)|$ instead of the Poisson integral to represent the solution in the continuous nonperiodic case.

Remark 2. Kernel (2.2) also has the advantage of avoiding the standard reduction to the continuous case via Poisson's summation formula by dealing with the symbol directly. This point of view will be beneficial when choosing the discretization in Section 3.

Remark 3. We point out that the choice of the kernel G is not unique. In fact, we could have obtained smoother kernels by modifying the symbol of G to, for instance,

$$\sum_{n=-\infty}^{\infty}\frac{\mathrm{e}^{-2\pi|k|y}}{(2\pi|k|)^p}\mathrm{e}^{2\pi\mathrm{i}kx}$$

for some power $p>1$ or more general symbols still. Here we only remark that an important feature of any possible alternative kernel is that it should contain all modes of decay as in the example chosen above. Appropriate "reflection properties" need also to be derived for the kernel in order to be able to define the symbol in the lower half plane. See Appendix B for more details about this.

Taking this perspective we can now introduce an associated boundary integral method and still recognize its relation to the Fourier method. This will be of utmost importance in the choice of the numerical scheme to actually preform the computations (see Sections 3 and 4).

2.2. A boundary integral method

Assume that the boundary curve Γ is parametrized by the periodic continuously differentiable function

$$s\in C^1([0,1),\mathbb{R}). \tag{2.17}$$

This assumption can be weakened but, since we are not interested in the optimal analytical result here, we shall not elaborate on that. Then we use kernel (2.2) and superpose translated copies of it along the curve Γ to obtain a x-periodic harmonic function u given by

$$u(x,y)=\int_0^1 G\Big(x-\tilde{x},y-s(\tilde{x})\Big)f(\tilde{x})\sqrt{1+s_x^2(\tilde{x})}\,\mathrm{d}\tilde{x} \tag{2.18}$$

for a suitable function $f\in L_{2,p}$. The latter is the Banach space of 1-periodic square integrable functions. If we choose the boundary function $g\in H^1_p$ with vanishing mean, then

$$\int_0^1 G\Big(x-\tilde{x},s(x)-s(\tilde{x})\Big)f(\tilde{x})\sqrt{1+s_x^2(\tilde{x})}\,\mathrm{d}\tilde{x}=g(x) \tag{2.19}$$

has a unique mean zero solution solution $f\in L_{2,p}$. We can then use (2.18) to obtain a boundary integral representation for $\mathrm{DtN}(g)$. Since

$$\nabla G(x,y)=\left(\frac{4\cos(\pi x)\sin(\pi x)}{2\cosh(2\pi y)-2\cos(2\pi x)},\frac{2-2\mathrm{e}^{-2\pi y}\cos(2\pi x)}{1+\mathrm{e}^{-4\pi y}-2\cos(2\pi x)\mathrm{e}^{-2\pi y}}-2\right) \tag{2.20}$$

and therefore

$$\nabla G(x,0)=\left(v.p.\frac{\cos(\pi x)}{\sin(\pi x)},\delta-1\right), \tag{2.21}$$

some care is needed in deriving the boundary integral representation. The result is contained in the following lemma.

Lemma 4. *Assume that $s\in C^1_p([0,1])$, then the following holds*

$$\begin{gathered}\int_\Gamma \partial_{\nu(z)}G(z-\tilde{z})f(\tilde{z})\,\mathrm{d}\sigma_\Gamma(\tilde{z})\\ \downarrow\\ -f(z_0)+v.p.\int_\Gamma \partial_{\nu(z_0)}G(z_0-\tilde{z})f(\tilde{z})\,\mathrm{d}\sigma_\Gamma(\tilde{z})\end{gathered} \tag{2.22}$$

as

$$(x,y)=z\to z_0=(x_0,s(x_0)),\quad (x,y)\in\Omega_\Gamma$$

if the limit is not taken tangentially to the boundary curve.

Proof. See Appendix A. □

We use the above formula in the discretizations of Section 3.

2.3. Decomposition of the integral equation

In this section, we present an analytic decomposition/factorization of Eq. (2.19) which will eventually be mimicked in the discretization. We introduce the symbols

$$a_0=(2\pi|k|)_{k\in\mathbb{Z}^*},\quad g_0=(1/2\pi|k|)_{k\in\mathbb{Z}^*}$$

corresponding to the operators on the flat periodic geometry, where we used the standard notation $\mathbb{Z}^*:=\mathbb{Z}\setminus\{0\}$. We further need the nonconstant coefficient symbol

$$\Big(g_s(k,x,\tilde{x})\Big)_{k\in\mathbb{Z}^*} \tag{2.23}$$

corresponding to the kernel appearing in (2.19). We refer to Appendix B for a formula (see (B.2) and (B.3)) and for its derivation. Denoting the Fourier transform by

$$(\mathscr{F}_{x\to k}u)(k) = \int_0^1 \mathrm{e}^{-2\pi\mathrm{i}kx}u(x)\,\mathrm{d}x, \quad k\in\mathbb{Z},$$

it is natural to decompose

$$\mathscr{F}^{-1}_{k\to\tilde{x}}g_s(\cdot,x,\tilde{x})\mathscr{F}_{x\to k}$$

as follows

$$\mathscr{F}^{-1}_{k\to\tilde{x}}g_0\mathscr{F}_{x\to k} + \mathscr{F}^{-1}_{k\to\tilde{x}}\Big[g_s(\cdot,x,\tilde{x}) - g_0\Big]\mathscr{F}_{x\to k}. \tag{2.24}$$

Following the procedure outlined in the previous subsection we utilize this decomposition in dealing with (2.19).

We shall see that most (numerical) ill-conditioning can essentially be confined to the constant coefficient term in this formulation and show how to get rid of it in a way which transforms (2.19) into an equation of second kind. From the analytical point of view we proceed as follows. Denote the integral operator with symbol b by $\mathrm{op}(b)$. Then (2.24) simply reads

$$\mathrm{op}(g_s) = \mathrm{op}(g_0) + \mathrm{op}(g_s - g_0)$$

it is easy to see that

$$\mathrm{op}(a_0)\mathrm{op}(g_s) = \mathrm{id} - I_\Gamma + \mathrm{op}(a_0)\mathrm{op}(g_s - g_0) \tag{2.25}$$

for

$$I_\Gamma(u) = \int_\Gamma u(\tilde{z})\,\mathrm{d}\sigma_\Gamma(\tilde{z}).$$

Therefore, if we restrict our attention to mean zero functions, as we do, (2.25) simply reads

$$\mathrm{op}(a_0)\mathrm{op}(g_s) = \mathrm{id} + \mathrm{op}(a_0)\mathrm{op}(g_s - g_0). \tag{2.26}$$

It turns out that this point of view is very beneficial when choosing the appropriate discretization to be used. In particular we base our discretization on the following "mixed" reformulation of (2.19) obtained using (2.26)

$$\mathrm{op}(a_0)g = f + \mathrm{op}(a_0)\int_0^1 k(x,\tilde{x})f(\tilde{x})\,\mathrm{d}\tilde{x} \tag{2.27}$$

for

$$K(x,\tilde{x}) = G\Big(x-\tilde{x}, s(x)-s(\tilde{x})\Big)\sqrt{1+s_x^2(\tilde{x})} - G(x-\tilde{x},0). \tag{2.28}$$

The above factorization of the operator essentially shows that, in order to solve (2.19), one can solve

$$\mathrm{op}(g_0)g = f$$

instead, that is, consider g and f as if they were defined on a flat domain, and subsequently apply a "bounded" correction to the result. Eq. (2.27) looks very much like an integral equation of the second

kind. Its kernel is not explicitly known, however, since it is given by the DtN value of $K(\cdot,\tilde{x})$ for $\tilde{x}\in(0,1)$.

Remark 5. It is an important observation that we do not need the boundary curve to be of graph type. In fact, if

$$(x,y):(0,1)\to\mathbb{R}^2,\quad \alpha\mapsto(x(\alpha),y(\alpha))$$

is the parametrization (with parameter interval normalized to $(0,1)$) of an admissible "periodic" curve Γ, that is, a, at least Lipschitz, curve with

$$x(0)=0,\quad x(1)=1,\quad y(1)=y(0),$$

we can use the corresponding boundary representations

$$\int_0^1 G(x(\beta)-x(\alpha),y(\beta)-y(\alpha))f(x(\alpha),y(\alpha))\sqrt{x_\alpha^2(\alpha)+y_\alpha^2(\alpha)}\,\mathrm{d}\alpha=g(x(\beta),y(\beta)) \tag{2.29}$$

to determine the intermediate function f and, since Lemma 4 remains valid for such curves, obtain

$$(\mathrm{DtN}_\Gamma g)(x(\beta),y(\beta))=-f(x(\beta),y(\beta))+v.p.\int_0^1 K(\beta,\alpha)f(x(\alpha),y(\alpha))\sqrt{\frac{x_\alpha^2(\alpha)+y_\alpha^2(\alpha)}{x_\alpha^2(\beta)+y_\alpha^2(\beta)}}\,\mathrm{d}\alpha \tag{2.30}$$

with

$$K(\beta,\alpha)=-x_\alpha(\beta)\partial_y G(x(\beta)-x(\alpha),y(\beta)-y(\alpha))+y_\alpha(\beta)\partial_x G(x(\beta)-x(\alpha),y(\beta)-y(\alpha)).$$

The same decomposition of the operator described above is possible and leads to numerical benefits in this case, too. We shall come back to this in the section dedicated to numerical experiments (see Examples 4 and 8).

3. The discretization

We now turn to the actual numerical computation of DtN. In doing so we follow the procedure outlined in the previous sections. We discretize the periodicity interval $[0,1)$ at equidistant points

$$x_j=(j-1)h,\quad j=1,\dots,2^m+1=:n\quad\text{for } h=2^{-m}\text{ and } m\in\mathbb{N}.$$

Having fixed the discretization we denote the Fast Fourier Transform of a vector $f\in\mathbb{C}^n$ by $\mathscr{F}_m f$. If we write $\mathscr{F}_m$ only, we mean the representation matrix of the FFT in the natural basis of $\mathbb{C}^n$. First we need to take a look at (2.27) in order to determine the intermediate vector f. We take

$$\mathrm{op}_m(a_0)=\mathscr{F}_m^{-1}(P_m a_0)\mathscr{F}_m \tag{3.1}$$

as a discretization of $\mathrm{op}(a_0)$ where of course

$$(P_m a_0)=\mathrm{diag}\Big[(2\pi|k|)_{|k|\leqslant 2^{m-1}}\Big].$$

Next we discretize the remaining integral operator in (2.27) by using the trapezoidal rule to obtain

$$A_m(j,k)=h\big(G\big(x_j-x_k,s_j-s_k\big)-G(x_j-x_k,0)\big),\quad j,k=1,\dots,2^m, \tag{3.2}$$

where $(s_j)_{j=1,\dots,2^m}$ is the discretization of the function s we use to describe the boundary of Γ. Taking into account the asymptotic behavior of G into the singularity (cf. (2.21)) and the logarithmic nature of G we compute the difference $A_m(j,k)$ as

$$A_m(j,k) = \frac{1}{2\pi}\log\left[1+\frac{a_m(j,k)}{b_m(j,k)}\right], \quad j \neq k$$

for

$$a_m(j,k) = e^{-4\pi(s_j-s_k)} - 1 = -2\left(e^{-2\pi(s_j-s_k)} - 1\right)\cos\left(2\pi(x_j - x_k)\right)$$
$$b_m(j,k) = 2 - 2\cos(2\pi(x_j - x_k))$$

and

$$A_m(j,j) = \frac{1}{2\pi}\log\left[1 + (s_x)_j^2\right]$$

on the diagonal. We end up with a discretized equation for the vector

$$\tilde{f}_j^m = f_j^m\sqrt{1+(s_x)_j^2}, \quad j = 1,\dots,2^m$$

in the form

$$(\mathrm{id}_m + \mathrm{op}_m(a_0)A_m)\tilde{f}^m = \mathrm{op}_m(a_0)g^m. \tag{3.3}$$

Remark 6. At first sight it might appear that a good reason for subtracting the flat term in (3.2) be that it helps taking care of the singularity on the diagonal. Although this is certainly true, another benefit is actually the significant reduction of the condition number. We refer the reader to the next section for numerical examples illustrating this fact. From the analytical point of view, we observe that

$$\mathrm{op}_m(a_0)A_m$$

can be viewed as the discretization of a bounded operator and we therefore do not expect a deterioration of its conditioning as the mesh becomes finer.

At this point we compute $\tilde{f}^m$ as

$$\tilde{f}^m = (\mathrm{id}_m + \mathrm{op}_m(a_0)A_m)^{-1}\mathrm{op}_m(a_0)g^m$$

and proceed with the computation of $\mathrm{DtN}(g)$. We need to evaluate integral (2.22) which we discretize by means of the spectral "alternating point" trapezoidal rule (see [15]). In order words let the kernel in (2.22) be discretized as

$$B_m(j,k) = h((s_x)_j,-1)\cdot\nabla G(x_j - x_k, s_j - s_k)$$

if

$$j - k = 1 (\mathrm{mod}\ 2)$$

and

$$B_m(j,k) = 0$$

otherwise. Then we compute

$$\mathrm{DtN}_m(g_m) = -f^m + \frac{B_m \tilde{f}^m}{\sqrt{1 + (s_x)_m^2}}. \tag{3.4}$$

4. Numerical examples

In this final section, we compute a few examples to illustrate the virtues of the method developed in the previous sections. In particular we also consider curves of large variation as well as nonsmooth curves. We consider two types of examples. In a first group of examples we choose different boundary functions s and obtain test boundary functions g by using combinations of the simple x-periodic harmonic functions

$$h_k(x, y) = \mathrm{e}^{-2\pi k y} \cos(2\pi k x). \tag{4.1}$$

These will provide a good test for the accuracy of our method. In the second type of examples we choose both the boundary function s and the boundary value g freely. We would not bother choosing mean zero boundary values g but take the numerical projection

$$P^m g^m = g^m - \frac{\sum_j g_j^m \sqrt{1 + (s_x)_j^2}}{\sum_j \sqrt{1 + (s_x)_j^2}}$$

instead, where we again discretized the integrals by the trapezoidal rule.

4.1. $\mathrm{op}_m(a_0)$ is a good preconditioner

Although the decomposition (2.27) of the DtN operator seems natural from the theoretical point of view, it might well be numerically ineffective. We shall show that it in fact is tremendously beneficial. It turns out that $\mathrm{op}_m(a_0)$ carries most of the ill-conditioning of the problem but poses no problem as a ΨDO with constant coefficients. To illustrate this fact we consider a series of examples. We obviously do not need to consider any boundary value to compute the condition number c_0 of

$$\mathrm{id}_m + \mathrm{op}_m(a_0) A_m, \tag{4.2}$$

which is the only matrix we actually need to invert in our procedure. If one needs to consider very fine grids the structure of (4.2) can be exploited in combination with an iterative method for the inversion: The pseudodifferential operator $\mathrm{op}_m(a_0)$ can be dealt with in Fourier space whereas the integral operator could be tamed by multipole expansions (cf. [12]).

In the following examples we choose

$$m = 6, 7, 8, 9, 10.$$

We compare the condition number c_0 of (4.2) with the condition number c_1 of the discretization matrix *badA* corresponding to the unmodified boundary integral equation (2.19) modulo the fact that we factor out the smallest eigenvalue which corresponds to the 1D kernel of the continuous operator. The boundary curves considered in Examples 1–4 (and then again in Example 5–8 again) are depicted in Figs. 2 and 3.

Example 1. Consider the smooth boundary curve given by

$$s = 0.8 + \tanh(2 + \sin(2\pi x)).$$

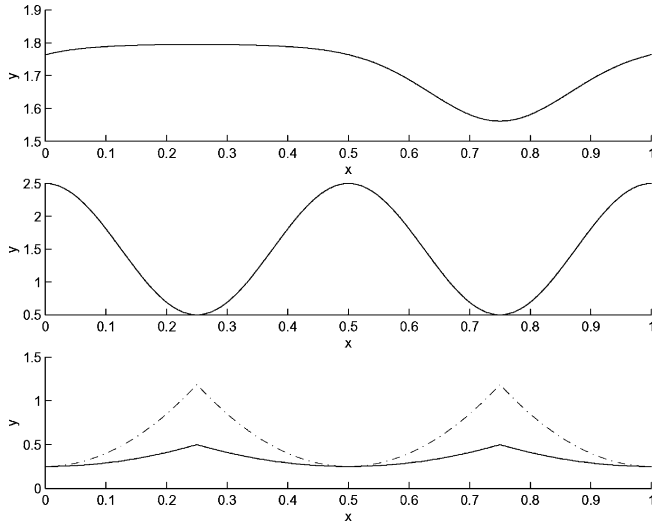

Fig. 2. The boundary curves Γ for Examples 1–3 and 5–7.

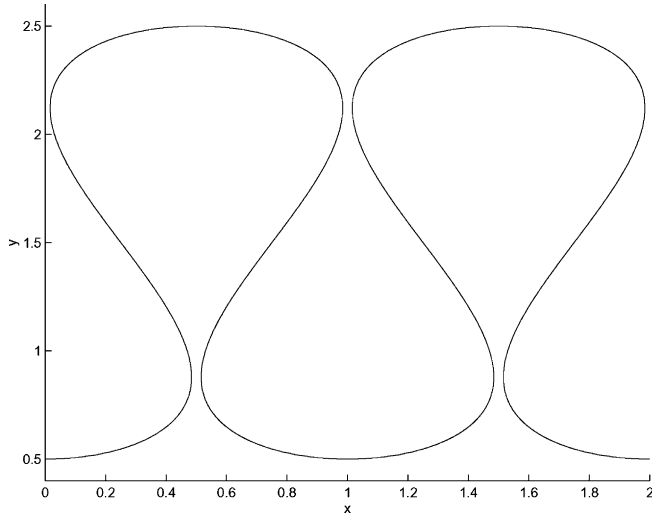

Fig. 3. Two periods of the boundary curve Γ for Example 4.

Table 1 contains the results obtained in this case.

Example 2. As a second example we take a curve s with a large variation given by

$$s = 0.5 + 2\cos^2(2\pi x).$$

Observe that the derivative of s roughly varies between -10 and 10. The results are summarized in Table 2.

Example 3. Finally we consider the nonsmooth Lipschitz curve

$$s = 0.25 + \alpha r$$

Table 1
The condition numbers for (4.2) and *badA*

	c_0	c_1
$m = 6$	1.5210	7.1795×10^2
$m = 7$	1.5210	2.0023×10^5
$m = 8$	1.5210	5.7463×10^5
$m = 9$	1.5210	1.2906×10^6
$m = 10$	1.5210	2.6674×10^6

Table 2
The condition numbers for (4.2)1 and *badA*

	c_0	c_1
$m = 6$	56.4739	3.6536×10^2
$m = 7$	56.4140	1.4635×10^3
$m = 8$	56.4139	2.5714×10^3
$m = 9$	56.4139	1.0205×10^4
$m = 10$	27.3285	3.4427×10^6

with

$$r = x^2\chi_{[0,0.25)} + (0.5 - x)^2\chi_{[0.25,0.75)} + (1 - x)^2\chi_{[0.75,1)},$$

where χ_J denotes the characteristic function of the interval J and $\alpha = 4, 15$. In this case the results for $\alpha = 4$ are found in Tables 3 and 4 for $\alpha = 15$.

Example 4. Finally, we consider the case of a curve Γ which can not be represented as the graph of a function (see Fig. 3). Let it be parametrized by

$$\gamma^1(x) = x + 0.35\sin(4\pi x), \quad \gamma^2(x) = 2 + \sin(2\pi(x - 0.25)), \quad x \in [0, 1].$$

Table 5 summarizes the results obtained in this case.

Table 3
The condition numbers for (4.2) and *badA*

	c_0	c_1
$m = 6$	2.4995	1.7830×10^3
$m = 7$	2.5822	3.4932×10^3
$m = 8$	2.6958	1.4214×10^4
$m = 9$	2.8223	5.6588×10^4
$m = 10$	2.9205	2.3298×10^5

Table 4
The condition numbers for (4.2) and *badA*

	c_0	c_1
$m = 6$	23.0605	7.3683×10^2
$m = 7$	24.5880	2.9023×10^3
$m = 8$	25.6142	8.6849×10^3
$m = 9$	9.2017	4.3001×10^4
$m = 10$	13.1765	1.8960×10^5

Table 5
The condition numbers for (4.2) and *badA*

	c_0	c_1
$m = 6$	48.1249	7.8616×10^1
$m = 7$	46.2576	7.9994×10^2
$m = 8$	46.2058	2.7657×10^3
$m = 9$	22.3886	1.1394×10^5
$m = 10$	12.9137	6.6306×10^5

It should be observed that the condition number of *badA* grows as the discretization becomes finer since the problem is ill-posed. Looking at the condition number c_0 we see that our preconditioning procedure really achieves its goal, since the condition number doesn't virtually grow anymore and is therefore all confined to the simple operator $\mathrm{op}_m(a_0)$. The second and third example suggest that a large variation in the boundary curve is actually worse that a lack of smoothness, at least in terms of the numerical properties. This is not completely unexpected since it becomes more and more difficult to capture the nonlocal contribution from different spots along the curve due to the fact that, in the large variation case, their contributions are many orders of magnitude apart from one another.

Remark 7. We point out that, eventhough the proposed preconditioning method is original, other preconditioning techniques have previously been used for single layer potentials in the context of boundary elements methods, see [6,10].

4.2. The method is very accurate

Next we take on the above examples again and actually compute the DtN operator and compare to the exact solution to illustrate the accuracy of the method we introduced. It should be clear that the method ought to be very accurate by construction. To show that we compute both the relative L_2 and the L_∞-norms. After that we compute DtN for generic curves and boundary data to show its stability with respect to variations of the domain geometry.

Let us fix

$$h(x,y) = \mathrm{e}^{-2\pi y}\cos(2\pi x) + 100\mathrm{e}^{-6\pi y}\cos(6\pi x) + \mathrm{e}^{-12\pi y}\cos(12\pi x)$$

as the harmonic function we use to produce the exact Neumann datum $\mathrm{DtN}(g)$ to the boundary value

$$g(x) = h(x, s(x)), \quad x \in [0,1) \tag{4.3}$$

along the boundary curve s. Let also

$$u = \mathrm{DtN}(g) \quad \text{and} \quad u_m = \mathrm{DtN}_m(g_m)$$

denote the exact and the approximate solution, respectively. We compute the relative $L_{2,p}(0,1)$ and $L_{\infty,p}(0,1)$-errors

$$e_m^2 = \frac{\|u - u_m\|_{L_2}}{\|u\|_{L_2}} = \sqrt{\frac{\sum_{j=0,\dots,n-1} |u(j*h) - u_m(j)|^2}{\sum_{j=0,\dots,n-1} |u(j*h)|^2}}$$

and

$$e_m^\infty = \frac{\|u - u_m\|_{L_\infty}}{\|u\|_{L_\infty}} = \frac{\max_{j\in\{0,\dots,n-1\}} |u(j*h) - u_m(j)|}{\max_{j\in\{0,\dots,n-1\}} |u(j*h)|}$$

Example 5. Assume that s is given as in Example 1 and that g is determined by (4.3). We obtain the results given in Table 6

Example 6. Consider now s as given in Example 2 and g given by (4.3). Then we obtain the errors contained in Table 7.

Example 7. Consider now s as given in Example 3 and g given by (4.3). The relative errors are given in Tables 8 and 9 for $\alpha = 4$ and for $\alpha = 15$, respectively.

Example 8. Consider now Γ as specified in Example 4 and g given by (4.3). We obtain the errors shown in Table 10.

Table 6
The relative error for s as in 1 and for (4.3)

	e_m^2	e_m^∞
$m = 6$	6.1303×10^{-9}	1.6655×10^{-8}
$m = 7$	4.2456×10^{-14}	1.1732×10^{-13}
$m = 8$	1.4749×10^{-13}	3.3107×10^{-13}
$m = 9$	4.5708×10^{-13}	9.6493×10^{-13}
$m = 10$	2.1229×10^{-12}	5.4297×10^{-12}

Table 7
The relative error for s as in 2 and for (4.3)

	e_m^2	e_m^∞
$m = 6$	8.9405×10^{-2}	1.0894×10^{-1}
$m = 7$	7.1529×10^{-3}	8.5876×10^{-3}
$m = 8$	3.8747×10^{-5}	5.1342×10^{-5}
$m = 9$	1.1816×10^{-9}	1.7387×10^{-9}
$m = 10$	1.7506×10^{-13}	9.9333×10^{-13}

Table 8
The relative error for s as in 3 and for (4.3)

	e_m^2	e_m^∞
$m = 6$	7.1434×10^{-6}	7.5789×10^{-6}
$m = 7$	1.3932×10^{-7}	1.9187×10^{-7}
$m = 8$	2.2859×10^{-9}	4.0785×10^{-9}
$m = 9$	3.4170×10^{-11}	9.1362×10^{-11}
$m = 10$	2.4456×10^{-12}	4.1165×10^{-12}

Table 9
The relative error for s as in 2 and for (4.3)

	e_m^2	e_m^∞
$m = 6$	4.7471×10^{-5}	5.3208×10^{-5}
$m = 7$	7.5167×10^{-10}	3.5195×10^{-10}
$m = 8$	2.5880×10^{-13}	3.6613×10^{-13}
$m = 9$	7.8558×10^{-13}	1.4393×10^{-12}
$m = 10$	3.2135×10^{-12}	6.1163×10^{-12}

Table 10
The relative error for s as in 2 and for (4.3)

	e_m^2	e_m^∞
$m = 6$	2.3240×10^{-3}	2.3202×10^{-3}
$m = 7$	1.0230×10^{-5}	1.4338×10^{-4}
$m = 8$	1.2225×10^{-6}	2.1721×10^{-6}
$m = 9$	1.4307×10^{-9}	2.8500×10^{-9}
$m = 10$	1.6602×10^{-13}	2.3675×10^{-13}

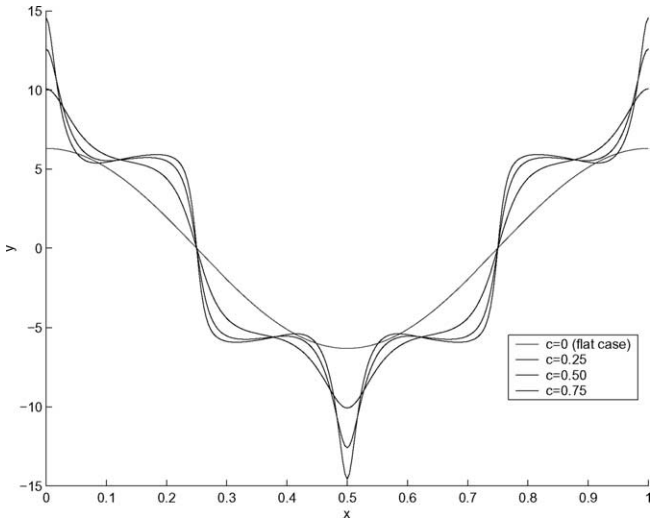

Fig. 4. The function $\mathrm{DtN}(cs, g)$ for different values of c.

The above examples show clearly that our method is very accurate, is stable in the sense explained and performs well even for curves which are nonsmooth and/or of large variation. The method appears to be spectrally accurate. Finally we would like to present an example where we freely choose both the curve s determining the boundary and the boundary datum g.

Example 9. Let us use s as given in Examples 2 and 6 and the boundary function

$$g(x) = \cos(2\pi x), \quad x \in (0, 1).$$

In Fig. 4 we show $\mathrm{DtN}(cs, g)$ for different values of $c \geqslant 0$ starting with the flat case for fixed discretization parameter $m = 8$.

5. Conclusion

We proposed a boundary integral method for the computation of the Dirichlet-to-Neumann operator in the 2D periodic case using ΨDO and explicit representations of the integral operators involved via periodic kernels. In the process we showed that there is a lot of freedom in the choice of the kernel to be used for the integral equations involved and how to produce appropriate periodic kernels solely by means of their flat symbols and the jump relation for their continuous counterparts. On this basis we suggested a discretization

method which works very well for curves which can be both nonsmooth and/or of large variation proving to be spectrally accurate. We proposed a preconditioning procedure for an integral equation of first kind which we therefore can accurately solve without resorting to special quadrature or regularization techniques. Finally we corroborated our analysis with a series of numerical examples which show the great benefits obtained.

The method developed here for the DtN operator appears very general and applicable to a variety of ill-posed integral equations. It also appears possible to use a similar procedure in 3D. We shall be addressing these issues in a forthcoming paper.

Acknowledgements

The author wishes to thank Hector Ceniceros for interesting discussions and helpful suggestions.

Appendix A

Proof of Lemma 4. Let R_α denote the rotation

$$R_\alpha = \begin{bmatrix} \cos(\alpha) & -\sin(\alpha) \\ \sin(\alpha) & \cos(\alpha) \end{bmatrix}$$

of angle $\alpha \in (-\pi/2, \pi/2)$ about the origin. We prove the claim for

$$(x_\varepsilon, y_\varepsilon) = (x_0, y_0) + \varepsilon R_\alpha(-s_x(x_0), 1) \in \Omega_\Gamma$$

letting $\varepsilon \to 0+$. Any general nontangential approximating sequence is in fact contained in a wide enough cone. Since the kernel is smooth away from the boundary curve we can consider

$$I_{0\leqslant\tilde{x}\leqslant 1}(\varepsilon) := \int_0^1 K(x,\tilde{x}) f(\tilde{x}) \sqrt{\frac{1+s_x^2(\tilde{x})}{1+s_x^2(x_0)}}\,\mathrm{d}\tilde{x}$$

for

$$K(x,\tilde{x},\varepsilon) = (s_x(x_0), -1)\cdot\nabla G(x_\varepsilon, y_\varepsilon).$$

Taking the limit as ε goes to 0 will produce the boundary value. The limit only exists on a regularity assumption for f. Here we think of f as being continuous but a natural assumption in the $L_{2,p}$ context would be $f \in H_p^{1/2}(\Gamma)$. We then split the integral into two pieces as follows

$$I_{0\leqslant\tilde{x}\leqslant 1}(\varepsilon) = I_{|x_0-\tilde{x}|\leqslant\sqrt{\varepsilon}} + I_{|x_0-\tilde{x}|>\sqrt{\varepsilon}}, \tag{A.1}$$

where the distance $|x_0 - \tilde{x}|$ is to be measured modulo the period, that is,

$$|x_0 - \tilde{x}| := x_0 - \tilde{x} \bmod 1.$$

Using (2.20) it is easily checked that

$$\nabla G(x,y) = \frac{1}{\pi}\left(\frac{x}{x^2+y^2}, \frac{y}{x^2+y^2}\right) + (r_1(x,y), r_2(x,y)) \tag{A.2}$$

for bounded functions r_i, $i = 1, 2$. It therefore follows that

$$I_{|x_0-\tilde{x}|>\sqrt{\varepsilon}}$$

$$\downarrow \quad (\varepsilon \to 0)$$

$$v.p. \int_0^1 K(x_0,\tilde{x}) f(\tilde{x}) \sqrt{\frac{1+s_x^2(\tilde{x})}{1+s_x^2(x_0)}} \mathrm{d}\tilde{x}$$

for

$$K(x_0,\tilde{x}) = -\partial_y G\Big(x_0-\tilde{x}, s(x_0)-s(\tilde{x})\Big) + s_x(x_0)\partial_x G\Big(x_0-\tilde{x}, s(x_0)-s(\tilde{x})\Big).$$

As to the first term in (A.1) we proceed as follows. Since f is smooth and $s_x \in C_p([0,1])$ it follows from (2.20) or (A.2) that

$$\int_{|x_0-\tilde{x}|\leqslant\sqrt{\varepsilon}} K(x_0,\tilde{x},\varepsilon)\left[f(\tilde{x})\sqrt{\frac{1+s_x^2(\tilde{x})}{1+s_x^2(x_0)}} - f(x_0)\right]\mathrm{d}\tilde{x}$$

converges to zero. Hereby we clearly set

$$K(x_0,\tilde{x},\varepsilon) = (s_x(x_0),-1)\cdot\nabla G(x_\varepsilon, y_\varepsilon).$$

We therefore only need to analyse

$$\int_{|x_0-\tilde{x}|\leqslant\sqrt{\varepsilon}} K(x_0,\tilde{x},\varepsilon) f(x_0)\,\mathrm{d}\tilde{x}.$$

Using (A.2) we see that

$$K(x_0,\tilde{x},\varepsilon) \approx -\frac{1}{\pi}\,\frac{-s(x_0)a_1(x_0,\tilde{x},\varepsilon)+a_2(x_0,\tilde{x},\varepsilon)}{a_1^2(x_0,\tilde{x},\varepsilon)+a_2^2(x_0,\tilde{x},\varepsilon)},$$

where

$$a_1(x_0,\tilde{x},\varepsilon) = x_0-\tilde{x}-\varepsilon[s_x(x_0)\cos(\alpha)+\sin(\alpha)]$$

and

$$a_2(x_0,\tilde{x},\varepsilon) = s(x_0)-s(\tilde{x})+\varepsilon[-s_x(x_0)\sin(\alpha)+\cos(\alpha)].$$

Now, taking into account the differentiability of s we obtain after some manipulation

$$K(x_0,\tilde{x},\varepsilon) \approx -\frac{1}{\pi}\,\frac{\varepsilon\cos(\alpha)}{(x_0-\tilde{x}-\varepsilon\sin(\alpha))^2+\varepsilon^2\cos^2(\alpha)}. \tag{A.3}$$

When we write $f \approx g$ we mean that $f-g$ is a at least integrable function. It is therefore an easy computation to see that

$$\lim_{\varepsilon\to 0+}\int_{|x_0-\tilde{x}|\leqslant\sqrt{\varepsilon}} K(x_0,\tilde{x},\varepsilon) f(x_0)\,\mathrm{d}\tilde{x} = -f(x_0)$$

follows from (A.3) provided $\alpha \in (-\pi/2,\pi/2)$. In conclusion, putting all the pieces back together we obtain the claimed formula. □

Appendix B. Kernel derivation from the flat symbol

In general one cannot expect to obtain explicit representations for the kernel like (2.2). It is therefore important and interesting to obtain a representation of the nonflat kernel in terms of the symbol of its flat counterpart.

The DtN operator in the flat case can be viewed as a ΨDO with constant coefficients and symbol

$$d_0 = (2\pi|k|)_{k\in\mathbb{Z}}$$

or, equivalently, the "boundary operator" of the operator family with symbols

$$d_0(\cdot, y) = \left(\begin{bmatrix} 2\pi i k \\ -2\pi|k| \end{bmatrix} \cdot \begin{bmatrix} 0 \\ -1 \end{bmatrix} e^{-2\pi|k|y} \right)_{k\in\mathbb{Z}}, \quad y > 0,$$

which corresponds to the symbol of the periodic Poisson kernel. It seems therefore natural to view the DtN operator for a generic curve as the ΨDO with nonconstant coefficients with symbol

$$d(\cdot, x, \tilde{x}) = \left(\begin{bmatrix} 2\pi i k \\ -2\pi|k| \end{bmatrix} \cdot \begin{bmatrix} v_1(x) \\ v_2(x) \end{bmatrix} e^{-2\pi|k|(s(x)-s(\tilde{x}))} \right)_{k\in\mathbb{Z}}, \quad x, \tilde{x} \in [0,1)$$

using the standard notation for ΨDOs (see [4] for instance) and denoting the unit outer normal to Γ at $x \in \Gamma$ with $v(x)$. The latter is simply the "normal derivative symbol" of

$$a(\cdot, x, \tilde{x}) = \left(e^{-2\pi|k|(s(x)-s(\tilde{x}))} \right)_{k\in\mathbb{Z}}, \quad x, \tilde{x} \in [0,1),$$

restricted to the boundary. The kernel

$$K(x, \tilde{x}) = H\left(x - \tilde{x}, s(x) - s(\tilde{x})\right), \quad x, \tilde{x} \in [0,1),$$

seems to be directly associated to this symbol via

$$K(x, \tilde{x}) = \sum_{k\in\mathbb{Z}} e^{-2\pi|k|(s(x)-s(\tilde{x}))} e^{2\pi i k(x-\tilde{x})}.$$

Unfortunately this point of view seems hopelessly formal in view of the terrible lack of convergence of the above series. The difference $s(x) - s(\tilde{x})$ can and, in fact, always will assume both positive and negative values unless the curve is flat. We now show how this point of view can be safely maintained with the necessary modifications.

Theorem 8. *The Fourier symbol of the operator with kernel K for a generic curve* (*of graph type*) *is given by*

$$a(k, x, \tilde{x}) = e^{-2\pi|k|(s(x)-s(\tilde{x}))}$$

if

$$k \in \mathbb{Z}, \quad x, \tilde{x} \in [0,1) \text{ s.t. } s(x) - s(\tilde{x}) \geqslant 0$$

and by

$$a(k, x, \tilde{x}) = -2\delta(k) - e^{2\pi|k|(s(x)-s(\tilde{x}))}$$

if

$$k \in \mathbb{Z}, \quad x, \tilde{x} \in [0,1) \text{ s.t. } s(x) - s(\tilde{x}) < 0.$$

Proof. Whenever the "natural" series converges it obviously sums up to

$$H\Big(x-\tilde{x}, s(x)-s(\tilde{x})\Big).$$

Now, H is also well-defined in the lower half plane and its values for negative second argument are precisely those we need to complete the definition of our symbol in the appropriate way. Fortunately, the values of H in the lower complex half-plane are uniquely determined by those in the upper half-plane. In fact H enjoys the symmetry property

$$H(x,-y)+H(x,y)=-2, \quad x\in\mathbb{R}, \ \ y>0. \tag{B.1}$$

Since H is known explicitly, this can be checked by a simple calculation. It is therefore clear how the symbol needs to be defined for

$$s(x)-s(\tilde{x})<0$$

in order to produce the right kernel. □

Remark 9. In most cases (like for the DtN operator in 3D) one cannot produce an explicit formula for the kernel. It is therefore crucial to understand how the definition of the "right symbol" has to be made based on available knowledge. The latter consists of the "convergent part" of the series and of the singularity in the origin, which coincides with the one of the continuous flat geometry kernel. The free space version of H is given by

$$H_f(x,y)=\frac{1}{\pi}\frac{y}{x^2+y^2}, \quad x\in\mathbb{R}, \ \ y\neq 0,$$

and satisfies the well-known jump-relation

$$\lim_{y\to 0\pm} H_f(x,y)=\pm\delta \text{ in } \mathscr{S}'(\mathbb{R}).$$

It follows directly from the Fourier series representation of H that

$$\lim_{y\to 0+} H(x,y)=\delta-1.$$

Since the jump-relation is determined by the singularity, which, in turn, is determined by the "continuous kernel" we obtain the following jump relation for the periodic kernel

$$\lim_{y\to 0\pm} H(x,y)=\pm\delta-1,$$

which leads to the symmetry property (B.1) in the limit as $y\to 0$. The property extends to the whole complex plane since $H(\cdot,\cdot)+H(\cdot,-\cdot)\equiv -2$ is the unique continuous bounded harmonic function with value -2 on the real line by Liouville's theorem.

The same analysis can be performed for the kernel G, given by (2.2). Its symbol is then seen to be given by

$$g(k,x,\tilde{x})=\frac{\mathrm{e}^{-2\pi|k|(s(x)-s(\tilde{x}))}}{2\pi k} \tag{B.2}$$

if

$$k\in\mathbb{Z}, \quad x,\tilde{x}\in[0,1) \text{ s.t. } s(x)-s(\tilde{x})\geqslant 0$$

and by

$$g(k,x,\tilde{x}) = \frac{e^{2\pi|k|(s(x)-s(\tilde{x}))}}{2\pi k} + e^{2\pi i k\tilde{x}}\hat{c}(k,\tilde{x}) \tag{B.3}$$

if

$$k \in \mathbb{Z}, \quad x,\tilde{x} \in [0,1) \text{ s.t. } s(x) - s(\tilde{x}) < 0,$$

where the correction term $\hat{c}$ is given by

$$\hat{c}(\cdot,\tilde{x}) = \mathscr{F}_{x\to k} c(\cdot,\tilde{x})$$

for

$$c(x,\tilde{x}) = -2\Big(s(x) - s(\tilde{x})\Big)\chi_{[s(x)-s(\tilde{x})<0]}$$

χ_S being the characteristic function of the set S.

References

[1] J.T. Beale, T.Y. Hou, J. Lowengrub, Stability of boundary integral methods for water waves, in: Nonlinear Evolutionary Partial Differential Equations (Beijing, 1993), AMS/IP Stud. Adv. Math., vol. 3, American Mathematical Society, Providence, RJ, 1997, pp. 1–7–127.

[2] J.T. Beale, T.Y. Hou, J.S. Lowengrub, Convergence of a boundary integral method for water waves, SIAM J. Numer. Anal. 33 (5) (1996) 1797–1843.

[3] R.R. Coifman, Y. Meyer, Nonlinear harmonic analysis and analytic dependence, in: F. Trèves (Ed.), Pseudodifferential Operators and Applications, Proceedings of Symposia in Pure Mathematics, vol. 43, American Mathematical Society, Providence, RJ, 1985, pp. 71–79.

[4] H.O. Cordes, The Technique of Pseudodifferential Operators, London Mathematical Society Lecture Note Series, vol. 202, Cambridge University Press, Cambridge, 1995.

[5] W. Craig, S. Sulem, Numerical simulation of gravity waves, J. Comput. Phys. 108 (1) (1993) 73–83.

[6] S.A. Funken, E.P. Stephan, The bpx preconditioner for the single layer potential operator, Appl. Anal. 67 (1997) 327–340.

[7] D. Givoli, Numerical Methods for Problems in Infinite Domains, Elsevier, Amsterdam, 1992.

[8] T.Y. Hou, J.S. Lowengrub, M.J. Shelley, Boundary integral methods for multicomponent fluids and multiphase materials, J. Comput. Phys. 169 (3) (2001) 302–362.

[9] F. John, Partial Differential Equations, Springer, New York, 1982.

[10] M. Kamon, M.J. Tsuk, J. White, Fasthenri: a multipole-accelerated 3-d inductance extraction program, IEEE Trans. Microw. Theory and Techniques (1994).

[11] A. Kirsch, An Introduction to the Mathematical Theory of Inverse Problems, Applied Mathematical Sciences, vol. 120, Springer, New York, 1996.

[12] A. McKenney, L. Greengard, A. Mayo, A fast poisson solver for complex geometries, J. Comput. Phys. 118 (2) (1995) 348–355.

[13] D.M. Milder, An improved formalism for electromagnetic scattering from a perfectly conducting rough surface, Radio Sci. 31 (6) (1996) 1369.

[14] D.P. Nicholls, F. Reitich, Stability of high-order perturbative methods for the computation of Dirichlet–Neumann operators, J. Comput. Phys. 170 (2001) 276–298.

[15] A. Sidi, M. Israeli, Quadrature methods for periodic singular and weakly singular Fredholm integral equations, J. Sci. Comput. 3 (1988) 201.

[16] M.E. Taylor, Tools for PDE, Mathematical Surveys and Monographs, vol. 81, American Mathematical Society, Providence, RJ, 2000.